

# A new semiempirical model of the peak electron density of the Martian ionosphere

Michael Mendillo,<sup>1</sup> Angela G. Marusiak,<sup>1</sup> Paul Withers,<sup>1</sup> David Morgan,<sup>2</sup> and Donald Gurnett<sup>2</sup>

Received 9 August 2013; revised 7 October 2013; accepted 9 October 2013; published 28 October 2013.

[1] Observations of the ionosphere of Mars have now reached a sufficient number to begin discussions on how best to create an empirically based model of its global morphology. Here we use nearly 113,000 values of maximum electron density ( $N_{\max}$ ) obtained from 2005 to 2012 by the Mars Advanced Radar for Subsurface and Ionospheric Sounding on board the Mars Express satellite. At the altitude of peak density, photochemical processes dominate over dynamical effects, and thus values of  $N_{\max}$  can be organized using three basic parameters: solar flux, solar zenith angle, and orbital distance. The model can be used retrospectively to provide  $N_{\max}$  values for any date starting in 1965. Forecasts are possible using predicted solar flux values extending to the end of solar cycle 24. Validations using Viking in situ observations and radio occultation measurements from several satellite missions provide encouraging results for a useful semiempirical climatological model. **Citation:** Mendillo, M., A. G. Marusiak, P. Withers, D. Morgan, and D. Gurnett (2013), A new semiempirical model of the peak electron density of the Martian ionosphere, *Geophys. Res. Lett.*, *40*, 5361–5365, doi:10.1002/2013GL057631.

## 1. Introduction

[2] The first generation of observations of Mars' ionosphere, distributed over ~13 years (1965–1978) [Mendillo *et al.*, 2003, Table 1], provided discovery mode information about the vertical structure of the Martian plasma environment. Yet these initial data sets were far too sparse to be used as the basis for an empirical global model. The second generation series of radio occultation experiments at Mars yielded a total of 5600  $N_e(h)$  profiles from the Mars Global Surveyor (MGS) satellite [Hinson *et al.*, 1999] and a continuing series of profiles from the European Space Agency's Mars Express (MEX) mission [Pätzold *et al.*, 2005]. The science yield from these observations has been substantial, ranging from descriptions of basic morphology to disturbances associated with solar flares, meteor impacts, and crustal magnetic fields (see reviews in Haider *et al.* [2011] and Withers [2009]). The geometrical constraints associated with most of these radio

occultation observations (high latitudes and high solar zenith angles) were still too restrictive for the specification of global morphologies.

[3] The MEX satellite has a second radio science instrument, the Mars Advanced Radar for Subsurface and Ionospheric Sounding (MARSIS). MARSIS has two distinct modes of radar operations—an Active Ionosphere Sounder (AIS) [Gurnett *et al.*, 2005] and a Subsurface radar mode [Picardi *et al.*, 2005]. The former measures the electron densities down to the height of maximum electron density ( $N_{\max}$ ); the second mode obtains the integral of the full electron density profile, called the total electron content (TEC). MARSIS observations can, in principle, be conducted at any time or location, and very large databases of  $N_{\max}$  and TEC are available to begin formulations of a global model of Mars' ionosphere.

## 2. Approach

[4] In this paper, we describe our attempt to construct a semiempirical model (meaning numerical parameterizations guided by theory of observed patterns) of the Martian ionosphere. The ideal approach would be to use observations of the full electron density profiles but, as described above, that is simply not possible from the limited distribution of samplings obtained from radio occultation methods. To create a baseline model of the Martian ionosphere, we decided to focus initially on  $N_{\max}$  as the parameter most descriptive of the magnitude of the ionosphere on any given day. This choice allows parameterizations of observed patterns to be approached using well-known and easily available photochemical parameters. These include the Sun's irradiance reaching Mars (represented by the solar radio flux proxy,  $F_{10.7}$ ) and the solar zenith angle (SZA) at the orbital distance ( $d$ ) of Mars on a specific day. Many previous studies have shown that  $N_{\max}$  [e.g., Němec *et al.*, 2011] and TEC [e.g., Lillis *et al.*, 2010] at Mars follow these parameters, as photochemical theory demands.

[5] A first attempt to create an observation-based model for Mars' ionosphere was presented in Němec *et al.* [2011] using the equations from basic Chapman Theory. In their formulation, attention was focused on altitudes at and above the height of  $N_{\max}$ . Observations came from MARSIS/AIS, as well as in situ plasma densities measured at the spacecraft altitude [Duru *et al.*, 2008], between August 2005 and December 2009. Their focus was on defining correction factors to Chapman Theory's  $N_e(h)$  profile parameters when observations were organized by their SZA and  $F_{10.7}$  values. Here we deal only with the peak electron density and use the photochemical equilibrium equation for a molecular ion/electron plasma, thus removing concerns about the inappropriate

<sup>1</sup>Center for Space Physics, Boston University, Boston, Massachusetts, USA.

<sup>2</sup>Department of Physics and Astronomy, The University of Iowa, Iowa City, Iowa, USA.

Corresponding author: M. Mendillo, Center for Space Physics, Boston University, 725 Commonwealth Ave. Rm. 506 Boston, MA 02215, USA. (mendillo@bu.edu)

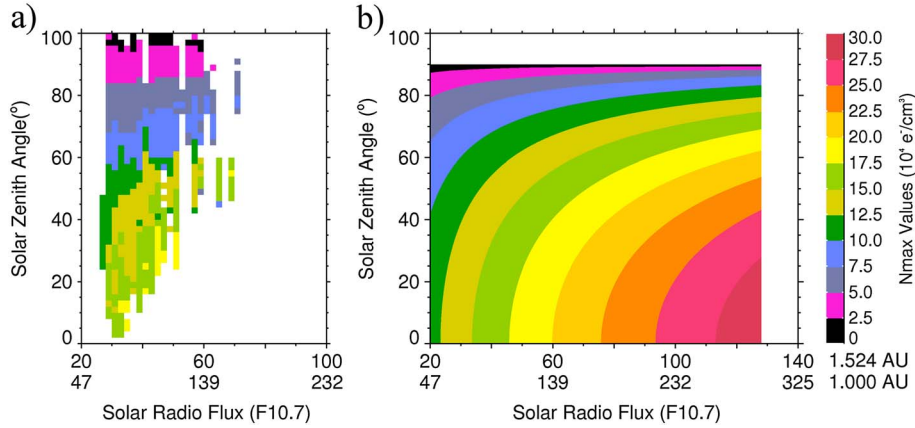


**Figure 1.** (a) Maximum Electron density ( $N_{\max}$ ) of Mars' ionosphere portrayed on a grid of solar zenith angle (SZ) and solar flux ( $F10.7$ ) at Mars' mean orbital distance of 1.524 AU. (b) A photochemical equilibrium solution of  $N_{\max}$  versus solar flux and SZ (equation 1, with flux =  $F10.7$ ) normalized by the data bin with the maximum number of observations (SZ =  $46^\circ$ ,  $F10.7 = 28$ ,  $N_{\max} = 11.4 \times 10^4 \text{ e}^-/\text{cm}^3$ ). Model predictions for high  $F10.7$  are to illustrate solar cycle effects.

assumptions within Chapman theory for the full electron density profile.

[6] The MARSIS/AIS data archive now has 112,718 values of  $N_{\max}$  spanning the years 2005–2012, thereby providing a more extensive set of observations (by a factor of  $\sim 3.5$ ) and a broader range of solar flux values than available at the time of the *Němec et al.* [2011] study. It is this database that we use to create a semiempirical ionospheric model for Mars.

### 3. Method

[7] For each of the MARSIS  $N_{\max}$  values, there is an associated UT date, solar zenith angle (SZ), solar flux ( $F10.7$ ), and distance from the Sun ( $d$  in AU). At the peak of the ionosphere where the plasma frequency is determined and the local electron density represents a balance between production and loss, there is a simple radial dependence on distance from the Sun ( $d$ ), i.e.,  $N_{\max} \sim 1/d$  [Mendillo et al., 2003]. The solar radio flux at 10.7 cm has long been used as a proxy for the EUV radiation responsible for  $N_{\max}$ . While direct measurements of solar irradiance at the appropriate wavelengths for photoionization are now available, our initial choice in model development is to continue to use  $F10.7$  since it is available for both retroactive validations (to 1965) as well as for predictions during the upcoming Mars Atmosphere and Volatile Evolution Mission (MAVEN, 2014).  $F10.7$  measurements at Earth are routinely adjusted via  $1/d^2$  to their values at 1 AU—thereby giving an index of pure solar activity. Using these two well-known radial dependences for photochemical processes, the  $F10.7$  solar fluxes at Earth and the MARSIS  $N_{\max}$  data at  $d$  were adjusted to their values at Mars' orbital mean distance (1.524 AU). In addition, the orbital longitude separation of Mars from Earth is used to determine the terrestrial date most appropriate (assuming solar rotation only changes) for the effective  $F10.7$  to use at the time of an observation at Mars. With these adjustments made, all of the  $N_{\max}$  data were then sorted by solar zenith angle and  $F10.7$  at 1.524 AU. The results appear in Figure 1a.

[8] The pattern of  $N_{\max}$  versus SZ and solar flux shown in Figure 1a represents a new aeronomic format for the portrayal

of a molecular ion plasma in photochemical equilibrium, and thus, some initial discussion is needed. The coverage is obviously not complete, but the highest values do appear where the SZ is small and the  $F10.7$  is high (shown by the bright yellow values). At high SZAs (top), the contours are essentially horizontal for all solar fluxes—showing the rapid transitions to low  $N_{\max}$  values that occur when the SZ approaches  $90^\circ$  (the dawn and dusk terminators). At low SZAs, the pattern is quite different—the contours take on a more vertical appearance (as shown in the dark green contour in the lower left)—indicating the daytime ionosphere getting more robust as solar fluxes increase. With confidence thus established that the MARSIS  $N_{\max}$  morphology is consistent with basic photochemical equilibrium (PCE) theory, the next step was to extend these partial trends in SZ and  $F10.7$  to their full range of possible values. The well-known PCE equation relating electron density to SZ and solar flux via square root dependences was weighted by the amount of data in each bin shown in Figure 1a to yield a smooth pattern for  $N_{\max}$  at 1.524 AU, given by

$$N_{\max}(\text{SZ}, \text{Flux}) = 2.58 \times \frac{10^4 \text{ e}^-}{\text{cm}^3} \times [\text{Flux} \times \cos(\text{SZ})]^{1/2} \quad (1)$$

[9] The results are presented in Figure 1b. One can see a reasonable representation of the partial pattern of data versus  $F10.7$  and SZ in Figure 1a by the full dependence climatology shown in Figure 1b. We stress that the extension of the model to very high solar fluxes is shown for illustration only; such conditions have been observed in the Earth's ionosphere but not yet at Mars.

### 4. Validation

[10] We first tested the model against individual measurements of  $N_{\max}$  made by the Viking landers and then with several radio occultation experiments spanning different levels of solar activity. In each case, the specific measurement date was used to determine the distance of Mars from the Sun. Then the solar rotation angle was found to relate the appropriate day for the  $F10.7$  value observed at Earth (adjusted to 1 AU) to use at Mars' average distance (1.524 AU). The resulting  $N_{\max}$  value for the SZ observed

**Table 1.** Summary of Model Predictions for Sample Data Sets

Date	Mission	SZA	RF at 1 AU	$N_{\max}$ Observed ( $10^4 e^-/cm^3$ )	$N_{\max}$ Predicted ( $10^4 e^-/cm^3$ )
20 July 1976	Viking Lander 1 <sup>a</sup>	43.5	70.2	10.3	10.3 ± 1.6
3 September 1976	Viking Lander 2 <sup>a</sup>	46.4	70.8	10.0	10.6 ± 1.6
12 December 2004	MEX Radio Occultation <sup>b</sup>	83	95.6	5	5.3 ± 1.1
12 December 2004	MGS Radio Occultation <sup>b</sup>	78	95.6	7.1	6.9 ± 1.4
24 May 1972	Mariner 9 <sup>c</sup>	76.3	162.8	9.9	9.2 ± 1.8
7 June 1972	Mariner 9 <sup>c</sup>	72.9	110.8	12	8.3 ± 1.7
6 June 1972	Mariner 9 <sup>c</sup>	73.2	114.3	10.4	8.4 ± 1.7
13 June 1972	Mariner 9 <sup>c</sup>	72.5	137.5	10.2	9.4 ± 1.8
<December 9, 2000- January 31, 2001>	MGS Radio Science <sup>d</sup>	<78.8>	170.9	8.5	8.4 ± 1.7
14 June 1965	Mariner 4 <sup>e</sup>	67	80.7	9.5	8.7 ± 1.7

<sup>a</sup>Hanson *et al.* [1977].

<sup>b</sup>Mendillo *et al.* [2011].

<sup>c</sup>Kliore *et al.* [1973].

<sup>d</sup>Bougher *et al.* [2004].

<sup>e</sup>Fjeldbo *et al.* [1966].

was then determined from Figure 1b, as given by equation 1; it was then adjusted via a  $1/d$  dependence to yield the model prediction. Table 1 gives the Viking 1 and 2 results together with a selection of radio occultation observations from several missions. In most cases, the model data agreement is acceptable, if not excellent, while two cases (consecutive days) from the Mariner 9 mission show disagreements of 25–50%.

[11] To quote uncertainty levels associated with the model, we returned to the basic data set used to derive it. As pointed out in Duru *et al.* [2008], the plasma frequency can be measured by MARSIS/AIS with an accuracy of about  $\pm 1\%$ , and thus uncertainties in  $N_{\max}$  are about  $\pm 2\%$ . This is always less than the standard deviations about the mean values of  $N_{\max}$  within the SZA- $F_{10.7}$  bins shown in Figure 1a. This prompted us to quote uncertainty ranges associated with the model using the observed  $\sigma$  (in percent) of the bin-by-bin mean values of  $N_{\max}$  in Figure 1a. As might be anticipated, the MARSIS  $\sigma$  (%) trend revealed a basic dependence upon the magnitude of  $N_{\max}$ . Using quantitative groupings of peak density in units of  $10^4 e^-/cm^3$ , we found that for  $N_{\max} > 16$ ,  $\sigma = 5\%$ ; for  $16 > N_{\max} > 10$ ,  $\sigma = 15\%$ ; for  $10 > N_{\max} > 4$ ,  $\sigma = 20\%$ , and for  $N_{\max} \leq 4$ ,  $\sigma = 30\%$ . These are the origins of the  $\sigma$  (%) values in Table 1. To illustrate how the full range of SZA would lead to different uncertainties, we show in Figure 2a the case of the Viking 2 lander. The abrupt changes in uncertainty come directly from the parameterization described.

[12] Figure 2b shows results from the model’s capability to predict  $N_{\max}$  for a future date: MAVEN’s Mars Orbit Insertion (MOI), approximated as 15 September 2014. To make pure predictions, an estimate of solar flux is needed, which the model takes from the NOAA predictions of monthly mean values for the remaining years of solar cycle #24 ([www.swpc.noaa.gov/SolarCycle/SC24](http://www.swpc.noaa.gov/SolarCycle/SC24)). For the uncertainty levels to associate with predictions, the model combines the uncertainties in  $F_{10.7}$  ( $130 \pm 9.0$ ) with its parameterization of  $N_{\max}$  variability (described above) to yield the somewhat higher uncertainty limits shown for MAVEN’s MOI date.

[13] A different type of validation opportunity comes from the nearly continuous observations made by the MGS radio occultation experiment from 1 November 2000 to 6 June 2001. This MGS “period 4” data set has the broadest span of SZAs ( $71.8^\circ$ – $86.9^\circ$ ) and has been used in several previous studies summarized in Haider *et al.* [2011]. We ran the

model for each of the 1572  $N_{\max}$  observations, and the data model comparisons are shown in Figure 3. There is good agreement between the climatological model’s peak densities and the actual  $N_{\max}$  values observed for most of the values below  $\sim 11 \times 10^4 e^-/cm^3$ . To explore why the model overestimates  $N_{\max}$  above a certain threshold, we plot in Figure 4a the same model data comparisons in a time series format, with data shown by gray dots and model results by the red dots. Figures 4b and 4c give the solar flux and SZA at Mars at the same times. As pointed out when discussing

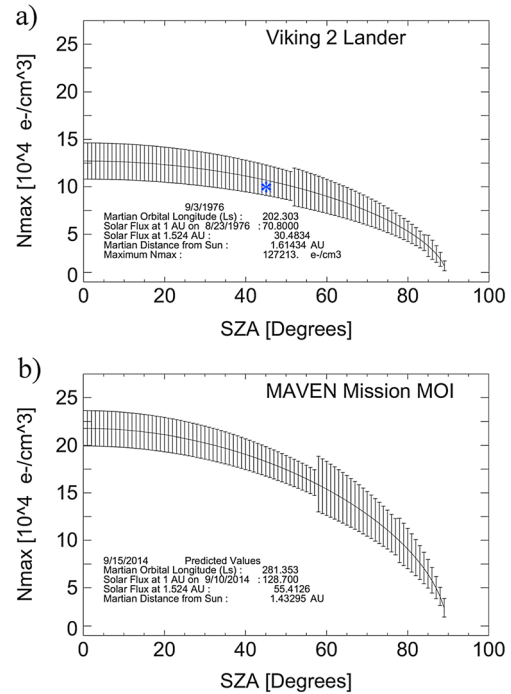


**Figure 2.** Examples of runs of the model for (a) a past date (the Viking 2 lander) and (b) a future date (MAVEN’s arrival at Mars). Both input and output parameters are shown, and the blue asterisk gives the  $N_{\max}$  value at the SZA of the Viking 2 lander. The uncertainty levels come from parameterizations of observed variabilities and for predictions of solar cycle  $F_{10.7}$  uncertainties (see text).

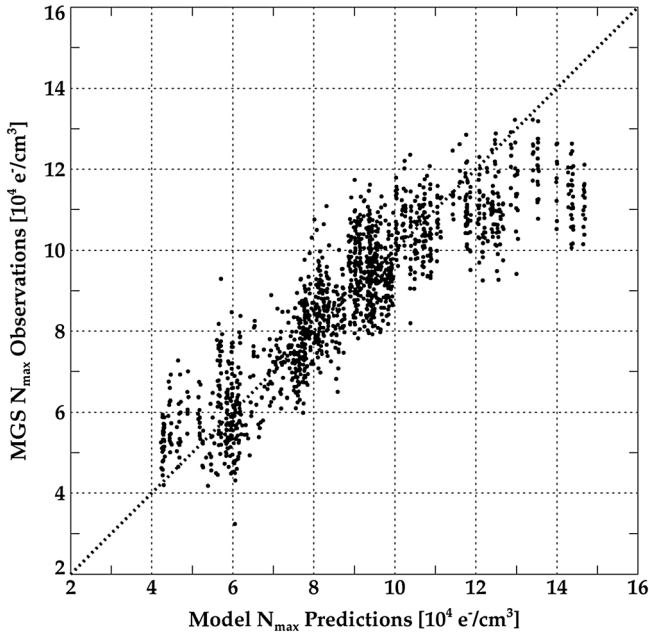


**Figure 3.** Comparison of model results with MGS observations of  $N_{\max}$  during a period of nearly continuous observations (November 2000 to June 2001). For a climatological model, agreement is acceptable except at the extremes of the diagonal line where the model underpredicts low values and overpredicts high values (see text).

Figure 1, the coupled dependence of  $N_{\max}$  upon SZA and  $F10.7$  separates at the extremes of SZA: for high SZA values (as with MGS period 4), SZA dominates; for low SZAs (not available from MGS observations), solar flux dominates. Thus, the overall  $N_{\max}$  morphology in Figure 4a is due to the SZA pattern in Figure 4c. The solar flux values are basically constant at  $\sim 60$   $F10.7$  units, except for short periods of solar variability. These include periods of low flux (early November and December) and more dramatic cases of high flux (late March and April). These are the points with maximum departures from the diagonal in Figure 3.

[14] The lack of robust correlations between ionospheric densities and solar flux proxies is a well-known statistical effect in terrestrial aeronomy. The linear correlations between  $F$  layer plasma and  $F10.7$  [e.g., Liu *et al.*, 2009] and the quadratic correlation between  $E$  layer densities and  $F10.7$  [Titheridge, 1997], break down when  $F10.7$  exceeds  $\sim 170$ – $180$  units. This effect is often called “saturation”—meaning that observed values are lower than predicted by high  $F10.7$  values. Physically, it points out that  $F10.7$  does not portray the ionizing wavelengths (EUV and X-rays) correctly over their full range of possible values [Richards *et al.*, 1994]. For a semiempirical model, a sudden increase in solar flux value can appear as a solar maximum irradiance acting upon a solar minimum background neutral atmosphere (thereby giving erroneous values). In reality, the atmosphere also adjusts to higher solar fluxes but not as instantaneously as photoionization occurs. The  $F10.7$  value of  $\sim 170$  units at 1 AU corresponds to  $\sim 75$  units at Mars’s mean distance, and Figure 4b shows this to be the case, i.e., the “saturation” effect in Figure 3 is due to the inability of a semiempirical model to handle solar active regions. Solutions adopted in terrestrial

aeronomy are as follows: (a) to add a constant to all  $F10.7$  values thereby lessening the impact of high values [Titheridge, 1997] or (b) to average a daily  $F10.7$  with its three solar rotation average [Richards *et al.*, 1994] to provide context for a specific daily value:

$$F_{\text{effective}} = \left[ \frac{(F10.7)_{\text{day}} + \langle F10.7 \rangle_{81\text{-day}}}{2} \right] \quad (2)$$

[15] Such a flux modification to our Mars model is shown by the blue dots in Figure 4a. The results are clearly in the correct direction, with the model’s low values being increased in November and December 2000, and its high values being decreased in March and April 2001. While the maximum values from the model no longer exceed actual observations, concerns remain, e.g., the time lag in response seen in the data for late March to early April, an effect not seen in the late April period; the model also overestimates  $N_{\max}$  during the rapidly changing SZAs in May to June. Within the context of Figure 3, equation 2 modification to the model results in the points at the lower left of the plot being moved to the right, while those at the upper end move to the left—in both cases falling closer to the diagonal. The formal statistic improvement in data model correlation using the Pearson correlation coefficients is from 0.88 to 0.91.

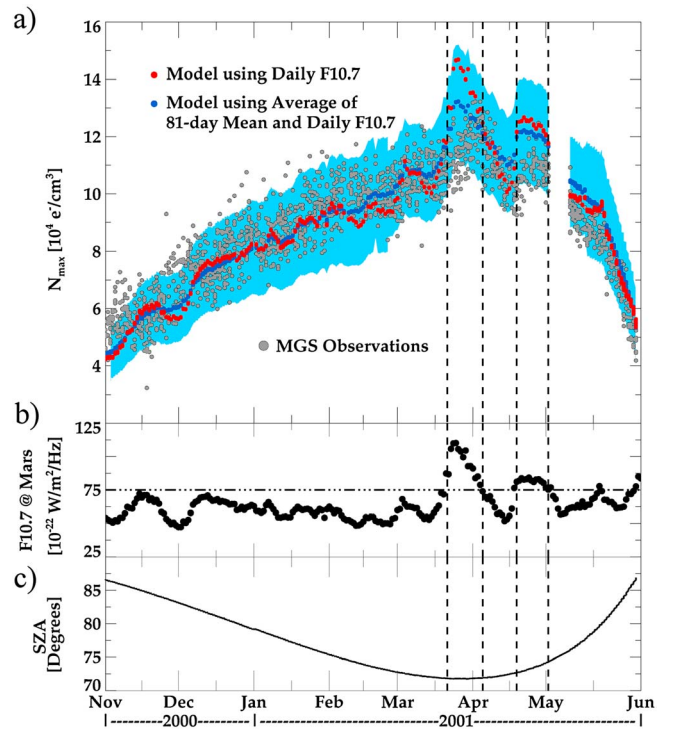


**Figure 4.** (a) Time series of the data and model results given in Figure 3 with simultaneous values of (b)  $F10.7$  and (c) SZA at Mars. Data points are shown in gray, with model results using equation 2 ( $\text{Flux} = F_{\text{effective}}$ ) in blue. Light blue shading portrays model uncertainties. The vertical dashed lines indicate the two time periods when  $F10.7 \geq 75$  units (see text).

## 5. Summary

[16] We have used a database of over 100,000 observations of the peak electron density of the ionosphere of Mars, spanning portions of solar cycles 23 and 24, merged with simple photochemical theory, to develop a first-order global model of Mars' ionosphere. Future validations and model improvements should include attempts to incorporate episodic effects due to dust storms, solar active regions, energetic particles, and coronal mass ejections. Additional challenges come from spatial sources of disturbance, e.g., crustal magnetic fields and topological features. As with terrestrial aeronomy, day-to-day variabilities driven by sources below the ionosphere (waves and tides) are the most difficult to include in a model.

[17] The present version of our model is called the Mars Initial Reference Ionosphere (MIRI Mark-1); it is available as a resource to use and to test via an interactive web site (<http://sirius.bu.edu/miri>). Users simply input a date, and MIRI generates a plot in the format shown in Figure 2 for either past or future dates. The authors welcome reports of model data comparisons, as well as comments and suggestions on ways to proceed.

[18] **Acknowledgments.** At Boston University, this work was supported, in part, by undergraduate student internship programs within the Center for Space Physics, by the comparative aeronomy component of NSF grant 1123222 (MM, PI) and by NASA MCDAP grant NMX12AJ39G (PW, PI). Undergraduates Trey Wenger and Gerard Lawler created the MIRI website and helped with the validations, respectively. Clara Narvaez helped with manuscript preparation and submission. The MARSIS/AIS program at the University of Iowa was supported by NASA through contract 1224107 with the Jet Propulsion Laboratory.

[19] The Editor thanks Hong Zou and an anonymous reviewer for their assistance in evaluating this paper.

## References

- Bougher, S., S. Engel, D. Hinson, and J. Murphy (2004), MGS Radio Science electron density profiles: Interannual variability and implications for the Martian neutral atmosphere, *J. Geophys. Res.*, *109*, E03010, doi:10.1029/2003JE002154.
- Duru, F., D. Gurnett, D. Morgan, R. Modolo, A. Nagy, and D. Najib (2008), Electron densities in the upper ionosphere of Mars from the excitation of electron plasma oscillations, *J. Geophys. Res.*, *113*, A07302, doi:10.1029/2008JA013073.
- Fjeldbo, G., W. Fjeldbo, and V. Eshleman (1966), Models for the atmosphere of Mars based on the Mariner 4 Occultation Experiment, *J. Geophys. Res.*, *71*, 2307–2316, doi:10.1029/JZ071i009p02307.
- Gurnett, D., et al. (2005), Radar sounding of the ionosphere of Mars, *Science*, *310*, 1929–1933, doi:10.1126/science.1121868.
- Haider, S., K. Mahajan, and E. Kallio (2011), Mars Ionosphere: A review of experimental results and modeling studies, *Rev. Geophys.*, *49*, RG4001, doi:10.1029/2011RG000357.
- Hanson, W., S. Sanatani, and D. Zuccaro (1977), The Martian ionosphere as observed by the Viking retarding potential analyzers, *J. Geophys. Res.*, *82*, 4351–4363, doi:10.1029/JS082i028p04351.
- Hinson, D., R. Simpson, J. Twicken, G. Tyler, and F. Flasar (1999), Initial results from radio occultation measurements with Mars Global Surveyor, *J. Geophys. Res.*, *104*, 26,997–27,012, doi:10.1029/1999JE001069.
- Kliore, A., G. Fjeldbo, B. Seidel, M. Sykes, and P. Woiceshyn (1973), S band radio occultation measurements of the atmosphere and topography of Mars with Mariner 9: Extended mission coverage of polar and intermediate latitudes, *J. Geophys. Res.*, *78*, 4331–4351, doi:10.1029/JB078i020p04331.
- Lillis, R., D. Brain, S. England, P. Withers, M. Fillingim, and A. Safaenili (2010), Total electron content in the Mars ionosphere: Temporal studies and dependence on solar EUV flux, *J. Geophys. Res.*, *115*, A11314, doi:10.1029/2010JA015698.
- Liu, L., W. Wan, B. Ning, and M. L. Zhang (2009), Climatology of the mean total electron content derived from GPS global ionospheric maps, *J. Geophys. Res.*, *114*, A06308, doi:10.1029/2009JA014244.
- Mendillo, M., S. Smith, J. Wroten, and H. Rishbeth (2003), Simultaneous ionospheric variability on Earth and Mars, *J. Geophys. Res.*, *108*(A12), 1432, doi:10.1029/JA00996.
- Mendillo, M., A. Lollo, P. Withers, M. Matta, M. Patzold, and S. Tellmann (2011), Modeling Mars' ionosphere with constraints from same-day observations by Mars Global Surveyor and Mars Express, *J. Geophys. Res.*, *116*, A11303, doi:10.1029/2011JA016865.
- Němec, F., D. Morgan, D. Gurnett, F. Duru, and V. Truhlik (2011), Dayside ionosphere of Mars: Empirical model based on data from the MARSIS instrument, *J. Geophys. Res.*, *116*, E07003, doi:10.1029/2010JE003789.
- Pätzold, M., S. Tellmann, B. Häusler, D. Hinson, R. Schaa, and G. Tyler (2005), A sporadic third layer in the ionosphere of Mars, *Science*, *310*, 837–839, doi:10.1126/science.1117755.
- Picardi, G., et al. (2005), Radar soundings of the subsurface of Mars, *Science*, *310*(5756), 1925–1928, doi:10.1126/science.1122165.
- Richards, P., J. Fennelly, and D. Torr (1994), EUVAC: A solar EUV flux model for aeronomic calculations, *J. Geophys. Res.*, *99*, 9981–9992.
- Titheridge, J. (1997), Model results for the ionospheric E region: Solar and seasonal changes, *Ann. Geophys.*, *15*, 63–78.
- Withers, P. (2009), A review of observed variability in the dayside ionosphere of Mars, *Adv. Space Res.*, *44*, 277–307, doi:10.1016/j.asr.2009.04.027.